

1 H2A ubiquitination is essential for Polycomb Repressive Complex 1-mediated gene regulation in

2 *Marchantia polymorpha*

3 Shujing Liu¹, Minerva S. Trejo-Arellano^{1,2}, Yichun Qiu¹, D. Magnus Eklund³, Claudia Köhler¹, Lars

4 Hennig^{1,4}

5 ¹Department of Plant Biology, Swedish University of Agricultural Sciences and Linnean Center for Plant

6 Biology, Uppsala 75007, Sweden.

7 ²Present address: Department of Cell and Developmental Biology, John Innes Centre, Norwich NR4 7UH,

8 UK

9 ³Department of Plant Ecology and Evolution, Evolutionary Biology Centre, Uppsala University, Uppsala

10 75236, Sweden

11 ⁴Deceased

12

13 Correspondence: Claudia.Kohler@slu.se

14

15

16

17

18

19

20 **Abstract**

21 Polycomb repressive complex 1 (PRC1) and PRC2 are chromatin regulators maintaining transcriptional
22 repression. The deposition of H3 lysine 27 tri-methylation (H3K27me3) by PRC2 is known to be required
23 for transcriptional repression, whereas the contribution of H2A ubiquitination (H2Aub) in the Polycomb
24 repressive system remains unclear in plants. We directly tested the requirement of H2Aub for gene
25 regulation in *Marchantia polymorpha* by generating point mutations in H2A that prevent ubiquitination
26 by PRC1. These mutants show reduced H3K27me3 levels on the same target sites as mutants defective in
27 PRC1 subunits MpBMI1 and the homolog MpBMI1L, revealing that PRC1-catalyzed H2Aub is essential
28 for Polycomb system function. Furthermore, by comparing transcriptome data between mutants in
29 *MpH2A* and *MpBMI1L*, we demonstrate that H2Aub contributes to the PRC1-mediated transcriptional
30 level of genes and transposable elements. Together, our data demonstrate that H2Aub plays a direct role
31 in H3K27me3 deposition and is required for PRC1-mediated transcriptional changes in both genic and
32 intergenic regions in *Marchantia*.

33

34

35

36

37

38

39

40

41

42 **Background**

43 Polycomb group (PcG) proteins are evolutionarily conserved epigenetic regulators which maintain
44 transcriptional gene repression in essential cellular and developmental processes in eukaryotes [1–4]. PcG
45 proteins typically belong to one of the two functionally distinct multi-protein complexes: Polycomb
46 Repressive Complex 1 (PRC1) and PRC2. PRC1 promotes chromatin compaction and catalyzes mono-
47 ubiquitination on histone 2A (H2Aub) mainly at lysine 119 in mammals, lysine 118 in *Drosophila*, and
48 lysine 121 in *Arabidopsis* [4–8], whereas PRC2 tri-methylates histone 3 at lysine 27 (H3K27me3) [9–12].
49 The catalytic core of the mammalian PRC1 is composed of the E3 ubiquitin ligases RING1A or RING1B
50 and one of six Polycomb RING finger (PCGF) proteins [13–15], while in *Drosophila* it consists of
51 RING1 (encoded by the *Sce* gene) and one of two PCGF proteins: Psc or Su(z)2 [16–18]. The
52 *Arabidopsis* PRC1 core includes AtRING1A or AtRING1B and one of the three AtBMI1s (homologs of
53 PCGF4) [6,19–21].

54 Previous studies on the Polycomb repressive system in *Drosophila* and mammals first proposed a PRC2-
55 initiated hierarchical model where PRC2 establishes H3K27me3, which is then recognized by
56 chromodomain-containing subunits of the canonical PRC1 (cPRC1). Nevertheless, later studies found this
57 classical hierarchical model not sufficient to explain the Polycomb repressive system [13,22,23]. Instead,
58 it was found that non-canonical PRC1 (ncPRC1) lacking chromodomain-containing subunits can recruit
59 PRC2 and establish stable Polycomb repressive domains [24–27]. This data point that the PRC1 catalytic
60 function is required for PRC2 recruitment, which was supported by recent work showing that in mouse
61 embryonic stem cells (ESCs), loss of RING1B catalytic activity largely phenocopies the complete
62 removal of the RING1B protein [28,29]. Nevertheless, whether this is a generally applicable concept
63 remains to be established. In *Drosophila*, H2AK118ub seems not required for repression of Polycomb
64 target genes during the early stages of embryo development and PRC2 binding to chromatin requires
65 PRC1 but not H2Aub [30,31]. Similarly, during neuronal fate restriction in mouse, PRC1 repression was

66 shown to function independently of ubiquitination of [32]. This data suggest that there are developmental
67 context-specific differences in the functional requirement of the catalytic activity of PRC1.

68 PRC1-catalyzed H2Aub has been intensively studied in *Arabidopsis thaliana*. H2Aub level, H3K27me3
69 incorporation and chromatin accessibility were shown to be affected by the depletion of components of
70 PRC1 [33–35]. Nevertheless, it remains unclear thus far whether H2Aub is required for H3K27me3
71 targeting. PRC1 is composed of multiple proteins that engage in interactions with PRC2 components.
72 Thus, AtRING and AtBMI1 in PRC1 can interact with LHP1, which co-purifies with PRC2 [19,20,36],
73 suggesting that PRC1 rather than H2Aub promotes H3K27me3 by interacting and recruiting PRC2 to
74 chromatin. H2Aub is associated with permissively accessible chromatin and the average transcription
75 levels of only-H2Aub marked genes are higher than that of H2Aub/H3K27me3 and only-H3K27me3
76 marked genes in *Arabidopsis* [33,35]. Consistently, removal of H2Aub is required for stable repression of
77 Polycomb target genes [34]. Together, based on current studies, the direct role of H2Aub in
78 transcriptional regulation remains unclear. To explore the functional role of H2Aub, we generated H2Aub
79 mutants by replacing the endogenous H2A by H2A variants with mutated lysines in the liverwort
80 *Marchantia polymorpha*.

81 *Marchantia* shares many signaling pathways with *Arabidopsis* and other seed plants [37]. Together with
82 its low genetic redundancy and possibilities to easily generate mutants, *Marchantia* is an ideal plant
83 model to study the evolutionarily conserved Polycomb system. There is only a single gene encoding
84 canonical H2A in *Marchantia*, compared to four genes in *Arabidopsis* [38]. We generated lysine to
85 arginine substitutions in H2A on residues K115/116/119 and demonstrate that all three lysines are
86 ubiquitinated *in vivo* and likely have redundant functions. We furthermore show that H2Aub mediates
87 H3K27me3 incorporation in both genic and intergenic regions in *Marchantia* and reveal that H2Aub is
88 essential for both, PRC1-mediated transcriptional activation and silencing.

89

90 **Results**

91 **H2Aub mediates H3K27me3 deposition on Polycomb target sites in genic and intergenic regions**

92 In mutants of PRC1 components, decreased H2Aub correlates with reduced H3K27me3 [33,35]. To
93 elucidate the functional requirement of H2Aub to induce H3K27me3 incorporation, we generated H2Aub
94 depleted lines by introducing point mutations in the potential ubiquitination sites of canonical MpH2A
95 (Fig. S1a). We co-transformed the point mutated *H2A* variants and a CRISPR construct designed to knock
96 out the endogenous *H2A* (Fig. S1b, S1c). Lysine 120 (K120) and K121 of *Arabidopsis* H2A were shown
97 to be ubiquitinated by AtBMI1 *in vitro* [6,20]; corresponding to K115 and K116 in MpH2A (Fig. 1a). In
98 *Drosophila*, mutations of four close lysine sites (K117, K118, K121 and K122) are required to abolish
99 total H2Aub [30]. We therefore generated *Mph2a;H2AK115R/K116R* and *Mph2a;H2AK119R* mutants
100 (jointly referred to as *h2a_ub* mutants) by substituting the C-terminal lysine residues K115 and K116 or
101 K119 of MpH2A with arginine. We failed to obtain *Mph2a* mutants expressing *H2A* variants with all
102 three point mutations, indicating that the three lysine sites of MpH2A are functionally redundant. The
103 global H2Aub level was strongly decreased in lines of *Mph2a;H2AK115R/K116R* and *Mph2a;H2AK119R*
104 mutants compared to wild type (WT) (Fig. 1b). Nevertheless, there was a remaining H2Aub signal in both
105 mutant lines, indicating that all lysine residues can be ubiquitinated *in vivo* and likely act redundantly.
106 The most obvious defects of *h2a_ub* mutants were downward curled edges of the thallus that grew into
107 the growth media and decreased gemmae dormancy compared to WT (Fig. 1c-1h).

108 To understand the connection between H2Aub and H3K27me3 in the Polycomb repressive system, we
109 generated ChIP-seq data for H3, H2Aub and H3K27me3 in WT, *Mph2a;H2AK115R/K116R* #1 and
110 *Mph2a;H2AK119R* #1 mutants. To validate our ChIP-seq data, we compared the H3K27me3 peaks in our
111 WT with previously published data [39]. The majority of peaks overlapped between both datasets (Fig.
112 S2), supporting the quality of our data. We found that genes with decreased H2Aub in the
113 *Mph2a;H2AK115R/K116R* mutant had also decreased H2Aub levels in the *Mph2a;H2AK119R* mutant,

114 but to a lesser extent (Fig. 1i). Conversely, genes with reduced H2Aub level in the *Mph2a;H2AK119R*
115 mutant were less affected in the *Mph2a;H2AK115R/K116R* mutant (Fig. 1j), supporting the notion that all
116 three lysine residues of MpH2A are targeted by ubiquitination. To test whether H3K27me3 deposition is
117 affected upon H2Aub depletion, we analyzed H3K27me3 on genes marked by either H2Aub or
118 H3K27me3 (all marked genes, all genes in Fig. 1k) and genes marked by both H2Aub and H3K27me3
119 (H2Aub/H3K27me3, overlapped genes in Fig. 1k). We found H3K27me3 levels to be decreased on all
120 marked genes and a more pronounced decrease on H2Aub/H3K27me3 genes in both *h2a_ub* mutants
121 compared to WT (Fig. 1l, 1m), revealing that H2Aub is essential for H3K27me3 deposition.

122 In *Marchantia*, 60% of H3K27me3 peaks are present in intergenic regions [39]; however, the location of
123 H2Aub peaks remains to be explored. Out of 6575 H2Aub peaks identified in WT, about 20% mapped to
124 intergenic regions, while most of the H2Aub peaks were located in gene body or promoter regions (Fig.
125 S3). We found intergenic regions covered by H2Aub and H3K27me3 also had decreased H3K27me3
126 levels in both *h2a_ub* mutants (Fig. 1n), revealing that H2Aub is required in intergenic regions to recruit
127 H3K27me3 in plants.

128

129 **H2Aub contributes to transcriptional activation**

130 Although many transcriptionally active genes are marked with H2Aub and H2Aub is associated with a
131 permissive chromatin state in *Arabidopsis* [33–35], it is unknown whether H2Aub is required for gene
132 activation. We noted that in *h2a_ub* mutants there were more downregulated than upregulated genes (Fig.
133 2a, 2b), suggesting that H2Aub has an activating role for gene expression in *Marchantia*. Both
134 upregulated and downregulated genes in *h2a_ub* mutants were enriched for genes with only-H2Aub and
135 H2Aub/H3K27me3 (Fig. 2c). We tested the H2Aub level on upregulated and downregulated genes in
136 *h2a_ub* mutants and found that H2Aub levels were decreased in the promoter regions of both gene

137 categories (Fig. 2d-2g), supporting that H2Aub contributes to gene repression as well as activation. We
138 also found more downregulated than upregulated TEs in *h2a_ub* mutants (Fig. 2h, 2i). There were 559
139 TEs marked with only-H2Aub, 1059 with H2Aub/H3K27me3 and 5728 with only-H3K27me3 (Fig. S4).
140 Among those, the only-H2Aub and H2Aub/H3K27me3 marked TEs had a significantly higher number of
141 highly transcriptionally active TEs than the only-H3K27me3 marked TEs (Fig. 2j), pointing that H2Aub
142 has the potential to activate TE expression and that removal of H2Aub is required for stable repression.

143

144 **MpBMI1/1L regulate morphological development of *Marchantia* and are involved in gene
145 repression and activation**

146 In *Arabidopsis*, AtBMI1s have been shown to be involved in H2A ubiquitination [6,20,21,33]. To explore
147 the extent to which MpBMI1/1L function relies on H2Aub, we generated MpBMI1 knock out mutants by
148 CRISPR/Cas9 in *Marchantia*. Using the AtBMI1A protein sequence as a query in a protein blast, we
149 identified two genes (*Mp7g12670* and *Mp6g09730* in the MpTak1 v5.1 annotation) encoding AtBMI1
150 homologs in *Marchantia*. MpBMI1, encoded by *Mp7g12670*, contains an N-terminal RING finger
151 domain and a C-terminal ubiquitin-like (RAWUL) domain [40], while *Mp6g09730* encodes for a protein
152 named MpBMI1-LIKE (MpBMI1L) that only has a C-terminal RAWUL domain. The RAWUL domain
153 is involved in protein-protein interaction and oligomerization of BMI1, which is essential for H2Aub
154 activity of PRC1 in mammals [41–44]. We generated *Mpbmi1/1l* double knockout mutants by
155 CRISPR/Cas9 and obtained combinations of double mutants with different mutations at the Cas9 target
156 sites (mutant information shown in Fig. S5, S6). Combinations of strong mutant alleles for both genes
157 *Mpbmi1-1/Mpbmi1l-1* (named *Mpbmi1/1l#1*, Fig. S5a) and *Mpbmi1-2/Mpbmi1l-2* (named *Mpbmi1/1l #2*,
158 Fig. S5b) caused strongly reduced growth rates and substantial size-reduction of gemma cups that
159 contained only few and smaller gemmae compared to WT (Fig. 3a-3c and 3f-3h). The slightly more
160 severe size reduction in *Mpbmi1/1l #1* compared to *Mpbmi1/1l #2* is likely due to the different extent of

161 deletions and insertions caused by CRISPR/Cas9 in these two lines (Fig. S5). We also obtained one
162 double mutant with a strong *Mpbmi1-3* allele and a weak *Mpbmi1l-3* allele (named *Mpbmi1/1l* #3, Fig.
163 S6a) and one *Mpbmi1l-4* single mutant (Fig. S6b), which showed weakly reduced growth rates compared
164 to WT (Fig. 3d, 3e). The fact that *Mpbmi1/1l* mutants had a more severe phenotype than *h2a_ub* mutants
165 is consistent with the proposed redundant function of ubiquitination on K115/K116 and K119 in H2A.
166 Western blot analysis revealed a global decrease of H2Aub in *Mpbmi1/1l* #1, *Mpbmi1/1l* #2 and
167 *Mpbmi1/1l* #3 double mutants compared to WT (Fig. 3i), with a more pronounced reduction in the
168 *Mpbmi1/1l* #1 mutant combination. We therefore used *Mpbmi1/1l* #1 in subsequent analyses. The residual
169 H2Aub signal in the *Mpbmi1/1l* mutants possibly reflects remaining functional activity of MpBMI1/1L
170 generated in the mutants. Alternatively, MpRING proteins have low functional activity in the absence of
171 MpBMI1/1L. We found 2085 genes being upregulated and 1023 genes being downregulated in the
172 *Mpbmi1/1l* mutants (Fig. 3j), suggesting that MpBMI1/1L mainly function as repressors, but also possibly
173 as activators. We analyzed H2Aub levels on the deregulated genes in the *Mpbmi1/1l* mutants and found
174 that H2Aub level significantly decreased on both upregulated genes and downregulated genes (Fig. 3k),
175 implying that H2Aub is required for MpBMI1/1L-mediated gene silencing and activation. Accordingly,
176 H2Aub marked genes were enriched in both upregulated and downregulated genes in *Mpbmi1/1l* mutants
177 (Fig. 3l).

178

179 **Ubiquitination of H2AK115/K116 and H2AK119 is required for PRC1-mediated gene and**
180 **transposable element expression**

181 To test whether impaired H2A ubiquitination and loss of PRC1 function has similar consequences, we
182 compared transcriptome data of the *Mph2a;H2AK115R/K116R* and *Mph2a;H2AK119R* mutants with that
183 of the *Mpbmi1/1l* mutants. Both *h2a_ub* mutants shared a significant number of upregulated genes (Fig.
184 4a) and we also found a significant overlap of upregulated genes between the *Mpbmi1/1l* mutants and

185 *h2a_ub* mutants (Fig. 4b, 4c) as well as between all mutants (Fig. 4d). Similarly, a significant number of
186 downregulated genes overlapped between two *h2a_ub* mutants and *Mpbmi1/1l* mutants (Fig. 4e-4h).
187 Genes commonly upregulated in *Mpbmi1/1l* and *Mph2a;H2AK115R/K116R* or *Mph2a;H2AK119R*
188 mutants were more strongly upregulated in *Mpbmi1/1l* than in the *h2a_ub* mutants (Fig. 4i, 4j),
189 supporting the idea that mono-ubiquitination on H2AK115/K116 and H2AK119 is functionally redundant
190 and mediated by MpBMI1/1L. Commonly downregulated genes in *h2a_ub* and *Mpbmi1/1l* mutants were
191 expressed at similar low levels in *h2a_ub* and *Mpbmi1/1l* mutants (Fig. 4k, 4l), consistent with the idea
192 that H2Aub is required for PRC1-mediated gene activation. Furthermore, it suggests that ubiquitination of
193 H2AK115/K116 and H2AK119 is not functionally redundant in activating gene expression. GO
194 enrichment analyses of upregulated genes overlapping between *Mpbmi1/1l* and
195 *Mph2a;H2AK115R/K116R* mutants (Fig. 4m) or *Mpbmi1/1l* and *Mph2a;H2AK119R* mutants (Fig. 4n)
196 both showed that response pathways were over-represented. Among downregulated genes overlapped
197 between *Mpbmi1/1l* and *h2a_ub* mutants we also found a significant enrichment for response pathway
198 related GOs (Fig. 5a, 5b), which were nevertheless largely distinct from the enriched GO terms of
199 upregulated genes.

200 The localization of H2Aub in intergenic regions indicated a role of this modification for transposable
201 element (TE) repression. Indeed, we identified more than 900 upregulated TEs in *Mpbmi1/1l* mutants, of
202 which a significant number overlapped with upregulated TEs in *h2a_ub* mutants (Fig. 5c-5e), revealing
203 that H2Aub is critical for PRC1-mediated TE silencing. Like for genes, commonly upregulated TEs
204 between *Mpbmi1/1l* mutants and *h2a_ub* mutants were more strongly upregulated in *Mpbmi1/1l* mutants
205 compared to *h2a_ub* mutants (Fig. 5f, 5g), pointing at redundant regulation of TEs by mono-
206 ubiquitination of H2AK115/K116 and H2AK119.

207

208 **H2Aub and H3K27me3 are affected in genic and intergenic regions by the depletion of MpBMI1/1L**

209 Consistent with the effect caused by AtBMI1 depletion in *Arabidopsis* [33], the H2Aub level was
210 significantly decreased on all marked genes as well as H2Aub/H3K27me3 genes in the *Mpbmi1/1l*
211 mutants compared to WT (Fig. 6a, 6b and S7a). Also the H3K27me3 level was significantly decreased on
212 all marked genes and H2Aub/H3K27me3 genes, yet not on only H3K27me3 genes in the *Mpbmi1/1l*
213 mutants compared to WT (Fig. 6c, 6d and S7b), implying that PRC1 activity mediates H3K27me3
214 deposition in *Marchantia*. Consistently, genes losing H2Aub showed significantly reduced H3K27me3
215 levels in the *Mpbmi1/1l* mutants compared to WT (Fig. 6e). We tested whether genes losing H2Aub in the
216 *Mpbmi1/1l* mutants belong to specific pathways. Among the top twenty significantly enriched GO terms,
217 nine GO terms correspond to multiple response pathways to intrinsic and extrinsic stimuli (Fig. 6f), which
218 occurred in the commonly upregulated and downregulated genes between *Mpbmi1/1l* mutants and *h2a_ub*
219 mutants. We tested whether the connection between H2Aub and H3K27me3 was restricted to genic
220 regions or was also present in intergenic regions. Loss of MpBMI1/1L caused a significant decrease of
221 both, H2Aub and H3K27me3 levels in intergenic regions (Fig. 6g-6i), revealing that PRC1-mediated
222 recruitment of PRC2 is not restricted to genic regions.

223

224 **Discussion**

225 Understanding the extent to which the function of histone modifying enzymes requires their catalytic
226 activity is an ongoing challenge in the chromatin field. While recent work revealed that the catalytic
227 activity of PRC1 is required in mouse ESCs [28,29], whether this requirement is evolutionary conserved,
228 remains to be demonstrated. We found that PRC1-catalyzed H2Aub contributes to the Polycomb-
229 mediated transcriptional repression in *Marchantia*, similar to the reported requirements in mouse ESCs
230 [28,29]. Our study thus supports an evolutionarily conserved Polycomb mechanism in plants and animals.

231 Loss of MpBMI1/1L activity in *Marchantia* impaired the genome-wide deposition of H3K27me3, similar
232 to reported findings in *Arabidopsis* [33]. Nevertheless, it was previously unknown whether the reduction

233 of H3K27me3 in *Atbmi1* is a consequence of decreased PRC1 catalytic activity or PRC1 non-catalytic
234 activity, since PRC1 and PRC2 were shown to interact [19,20,36]. By comparing the H2Aub deficient
235 mutants *Mph2a;H2AK115R/K116R* and *Mph2a;H2AK119R* with *Mpbmi1/l* mutants, we discovered that
236 reduction of H3K27me3 levels on Polycomb target genes in *Mpbmi1/l* mutants also occurred in *h2a_ub*
237 mutants that evade ubiquitination, demonstrating that H2Aub directly affects H3K27me3 deposition.
238 Previous work showed that PRC1 initiates silencing, followed by PRC2-mediated H3K27me3 that
239 maintains stable repression in *Arabidopsis* [6,21,33,34]. Our data add support to this model and extend it
240 by showing that the PRC1-mediated H2Aub is required for the initial PRC2-mediated repression.

241 In *Marchantia*, H3K27me3 is located in heterochromatic regions and marks TEs and repeats [39],
242 contrasting its mainly genic localization in *Arabidopsis* [33]. We show that PRC1-catalyzed H2Aub is
243 required for TE repression in *Marchantia*, revealing an ancestral role of the Polycomb system in TE
244 repression. Similarly, in *Drosophila*, H2AK118ub is widely distributed in intergenic regions and
245 depletion of PRC1 or PRC2 causes a genome-wide increase of transcriptional activity in intergenic
246 regions [45].

247 The failure to obtain *Mph2a;H2AK115R/K116R/K119R* mutants with complete loss of H2Aub strongly
248 suggests that H2Aub has essential functions in *Marchantia*. Similarly, H2Aub deficient *Drosophila*
249 embryos arrest at the end of embryogenesis, indicating that the requirement of H2Aub to regulate
250 essential biological functions is evolutionary conserved [30]. As for H2Aub deficiency, also loss of the
251 RING1 encoding gene *Sce* causes arrest of embryo development in *Drosophila* [30]. In contrast, we found
252 that mutants in *MpBMI1/l* are viable and similarly, also mutants in *Arabidopsis* BMI encoding genes are
253 viable [21]. Nevertheless, it is possible that in both systems BMI function is not completely depleted,
254 since the *Atbmi1b* and *Atbmi1c* mutant alleles are probably not complete null alleles [6,20] and we found
255 remaining H2Aub present in *Mpbmi1/l* mutants (Fig. 1g), pointing that the alleles have residual activity.
256 We failed to obtain CRISPR/Cas9 mutants using guide RNAs targeting an N-terminal region in the
257 *MpBMI1*, suggesting that complete loss of PRC1 function is lethal. Nevertheless, it is also possible that

258 RING proteins can have catalytic activity independent of BMI proteins, as suggested based on *in vitro*
259 catalytic activity of AtRING1A and AtRING1B proteins (Bratzel et al., 2010). Previous work revealed
260 that the H2A variant H2A.Z can be ubiquitinated in *Arabidopsis* and incorporation of this modification is
261 required for H2A.Z-mediated transcriptional repression [46]. It is possible that MpBMI1/1L also affects
262 ubiquitination of the H2A variant H2A.Z; which could provide an alternative explanation for the more
263 severe phenotype of *Mpbmi1/l* mutants compared to *h2a_ub*. Due to the lack of a suitable antibody, this
264 possibility could not be tested.

265 Previous work revealed that PRC1-mediated H2Aub1 is associated with chromatin responsiveness in
266 *Arabidopsis* and that responsive genes require H2Aub to initiate PRC2 mediated repression [34,35]. At
267 the same time, for stable gene repression H2Aub needs to be removed by the H2A deubiquitinases
268 UBP12 and UBP13, likely because the occurrence of H2Aub allows recruitment of the H3K27me3
269 demethylase REF6 (Kralemann et al., 2020). The association of H2Aub with gene activation is also
270 supported by our study, where we found more downregulated genes than upregulated genes in the *h2a_ub*
271 mutants and a high number of downregulated genes in *Mpbmi1/l* mutants. A significant number of
272 downregulated genes overlapped between the mutants, suggesting that the catalytic activity of PRC1 is
273 required for gene activation. How PRC1 activity connects to gene activation remains unclear, despite
274 several studies reporting the co-occurrence of ncPRC1 and active genes in mammalian systems [47–50].
275 It was proposed that the PRC1-catalytic activity may be dispensable for PRC1 function in promoting the
276 expression of active genes in mammalian systems [51]; however, our data rather suggest that PRC1-
277 catalyzed H2Aub is required for gene activation. We speculate that the role of H2Aub in gene activation
278 is connected to its proposed role in recruiting REF6 [34], an exciting hypothesis that remains to be tested.

279

280 **Conclusions**

281 In summary, we show that the ubiquitinated lysines in MpH2A act redundantly and H2Aub directly
282 contributes to the deposition of H3K27me3 in *Marchantia*, demonstrating the determinant role of PRC1
283 catalysis in the Polycomb repressive system. Together with previous findings in *Arabidopsis* and mouse
284 ESCs [28,29,33], our study supports an evolutionarily conserved Polycomb mechanism in divergent land
285 plants and animals. Our finding strongly support a model in which the catalytic activity of PRC1 is
286 required for PRC2-mediated gene repression and at the same time required for PRC2-independent gene
287 activation.

288

289 **Methods**

290 *Plant material and growth conditions*

291 *Marchantia polymorpha* ssp. *ruderaria* Uppsala accession (Upp) was used as WT and for transformation
292 [52]. Plants were grown on vented petri dishes containing Gamborg's B5 medium solidified with 1.4%
293 plant agar, pH 5.5, under 16/8 h photoperiod at 22°C with a light intensity of 60-70 $\text{umol m}^{-2} \text{ s}^{-1}$. Plate
294 lids were taped to prevent loss of water.

295

296 *Generation of DNA constructs*

297 Vectors pMpGE_En03, pMpGE010, pMpGWB401 and pMpGWB403 used in this study were previously
298 described [53,54]. DNA fragments used to generate the guide RNAs against *MpBMI1* and *MpBMI1L*
299 were prepared by annealing two pairs of primers (LH4513/LH4514, LH4517/LH4518, specified in table
300 S1). The fragments were inserted into the BsaI site of pMpGE_En03 to yield pMpGE_En03-
301 MpBMI1gRNA02 and pMpGE_En03-MpBMI1LgRNA04, respectively, and then transferred into
302 pMpGE010 and pMpGWB401 using the Gateway LR reaction (Thermo Fisher Scientific) to generate

303 pMpGE010_MpBMI1gRNA and pMpGWB401_MpBMI1LgRNA. Similarly, the two pairs of primers
304 (LH4012/LH4013, LH4303/LH4304) were used to generate pMpGE_En03-MpH2AgRNA2 and
305 pMpGE_En03-MpH2AgRNA3, which were subsequently transferred into pMpGE010 to generate
306 pMpGE010-MpH2AgRNA2 and pMpGE010-MpH2AgRNA3, respectively. H2AK115R/K116R and
307 H2AK119R were amplified by two pairs of primers (LH3848/LH4309 and LH3848/LH3849) and sub-
308 cloned into the pENTR-TOPO vector (Thermo Fisher Scientific) to generate pENTR-H2AK115R/K116R
309 and pENTR-H2AK119R, respectively. The pENTR vectors were transferred into pMpGWB403 by
310 Gateway LR reaction to yield pMpGWB403-H2AK115R/K115R and pMpGWB403-H2AK119R.
311 Primers used are listed in supplemental table S1.

312

313 *Generation of transgenic Marchantia polymorpha*

314 The constructs were transformed into spores of *Marchantia* by Agrobacterium GV3101 as described
315 previously [55]. Spores were grown in liquid Gamborg's B5 medium with 2% sucrose, 0.1% Casamino
316 acids and 0.03% L-Glutamine for 10 days under constant light. Agrobacteria containing constructs were
317 grown in liquid LB with antibiotic for two days and then pelleted. The pellet was resuspended in the spore
318 growth media with 100 mM acetosyringone and grown for 4 h at 28°C with spinning. Agrobacteria
319 suspension was added to spores together with acetosyringone to a final concentration of 100 mM and the
320 mixture was grown for another two days. Sporelings were plated on selection media with 200 mg/ml
321 Timentin. Several independent primary transformants (T1 generation) were analyzed for the presence of
322 the transgene by genomic PCR.

323

324 *Antibodies*

325 The antibodies used were anti-H3 (07-690, Merck Millipore, Burlington, MA, USA), anti-H2Aub
326 (#8240S, Cell signalling technology, Danvers, MA) and anti-H3K27me3 (07-449, Merck Millipore).

327

328 *Histone extraction and western blotting*

329 Histone extraction and western blotting of 15d seedlings were performed as previously described [36].

330

331 *RNA sequencing*

332 50 mg of 15 day-old thalli of WT, *Mpbmi1/1l*, *Mph2a;H2AK115R/K116R* and *Mph2a;H2AK119R*
333 mutants were used for RNA extraction. RNA was extracted using the MagMAX™ Plant RNA Isolation
334 Kit (Thermo Fisher Scientific) in biological triplicates. Libraries were generated using DNA-free RNA
335 with the NEBNext® Ultra™ II RNA Library Prep Kit for Illumina according to manufacturer's
336 instructions. Sequencing was performed on an Illumina HiSeq2000 in 150-bp pair-end mode at Novogene
337 (Hong Kong).

338

339 *Transcriptome data analysis*

340 Untrimmed reads were mapped to the *Marchantia polymorpha* MpTak1 v5.1 reference genome [39] using
341 STAR (v2.5.3.a, [56]). Read numbers of mapping statistics are reported in supplementary table S2.
342 Expression counts were generated using the R function summarizeOverlaps from the package HTSeq in
343 union mode on exons from the reference transcriptome MpTak1v5.1_r1. A comparison of RPKM in
344 RNA-seq triplicates showed high reproducibility of data in Fig. S8. Differential expression analyses were

345 performed using the R package DESeq2 (v1.20.0, [57]). Genes with an absolute log2 fold change ≥ 1 and
346 FDR ≤ 0.05 were considered as differentially expressed.

347

348 *H3, H2Aub1 and H3K27me3 ChIP-seq*

349 For H3, H2Aub, and H3K27me3 ChIP-seq, WT, *Mpbmi1/1l*, *Mph2a;H2AK115R/K116R* and
350 *Mph2a;H2AK119R* plants were grown for 15 days on B5 medium, and then about 300 mg thalli were
351 harvested. ChIP was performed as described before [58]. In short, vacuum infiltration with formaldehyde
352 was performed for 2x10 minutes. Crosslinking was quenched by adding glycine to a final concentration of
353 0.125 M under another 5-minute vacuum infiltration. Sonication of the chromatin was done for eight 30-s
354 ON, 30-s OFF cycles. Overnight antibody binding was performed directly after sonication, followed by
355 adding washed protein A dynabeads (Thermo Fisher Scientific) to each ChIP aliquot. De-crosslinking and
356 subsequent DNA recovery steps were performed using the Ipure kit v2 (Diagenode, Liège, Belgium). The
357 Ovation Ultralow Sytem V2 (NuGEN, Redwood city, CA, USA) was used for the ChIP-seq library
358 preparation, and 150 bp paired-end sequencing was performed on the HiseqX platform at Novogene
359 (Hong Kong). The ChIP-seq experiments were done using two biological replicates per IP, per genotype.

360

361 *Quality control and read mapping for ChIP-seq*

362 FastQC (<https://www.bioinformatics.babraham.ac.uk/projects/fastqc/>) was used to examine read quality
363 of each sample. Low quality ends (phred of <20) and adapter sequences were removed with Trimmomatic
364 (v0.39, [59]). Reads with low average quality were also discarded (phred < 28). For all experiments, reads
365 were mapped to the *M. polymorpha* reference genome MpTak1v5.1 using bowtie2 (v2.3.5.1; [60]).

366 Details on read numbers can be found in supplemental table S3. Genome sequence and gene annotation
367 data were downloaded from the *Marchantia* website (marchantia.info).

368

369 *Peak calling*

370 H2Aub and H3K27me3 aligned .sam files were imported into Homer [61]. Duplicated mappings were
371 removed using Homer. Peak calling was done using Homer with histone style settings and using histone
372 H3 as the background to control for nucleosome occupancy. The same analysis was performed with the
373 published WT H3K27me3 data (SRA: PRJNA553138) in *Marchantia* [39]. The peak tag counts were
374 generated by Homer. A comparison of normalized peak tag counts (RPKM) by Homer in ChIP-seq
375 replicates showed high reproducibility of data in Fig. S9. Only peaks present in both replicates of ChIP-
376 seq data were considered as real peaks and retained for subsequent analyses. Peaks were correlated with a
377 gene when the peaks were located at any region of this gene or at most 2 kb upstream of its transcription
378 start site. Lists of genes defined by the presence of H2Aub and H3K27me3 are shown in supplemental
379 table S4. Intergenic regions covered by H2Aub and H3K27me3 are listed in supplemental table S5. The
380 statistical comparison of differential peak tag counts was performed with DEseq2 package in R using the
381 raw tag counts outputs from Homer. Peaks with the adjusted p-value (FDR) < 0.05 were considered as
382 differentially changed peaks.

383

384 *Peak visualization*

385 Peak profiles were visualized by the Integrative Genome Viewer (IGV) [62]. Bigwig files were outputted
386 from “bamCoverage” function in deepTools [63] using Reads Per Kilobase Million (RPKM) as
387 normalization parameter. The Bigwig files were further used in the “computeMatrix” function in

388 deepTools with the “scale-regions” as setting parameter to generate H2Aub and H3K27me3 matrix on
389 genes from 3 kb upstream of the transcriptional start to 3 kb downstream of the transcriptional end of
390 genes, with a bin size of 50 bp. H2Aub and H3K27me3 scores (RPKM) of genes in boxplots were
391 calculated as the average RPKM from 2 kb upstream of the transcriptional start to the transcriptional end
392 of genes. H2Aub and H3K27me3 levels (RPKM) in intergenic region in boxplots were normalized tag
393 counts about intergenic peaks generated from reads files (.sam file) during peak calling by Homer.

394

395 *GO analysis*

396 GO analyses were performed on the *Arabidopsis* homologs of *Marchantia* genes. The homologs of
397 *Marchantia* genes in *Arabidopsis* were retrieved from PLAZA 4.0 DICOT, inferred by the Best-Hits-and-
398 Inparalogs (BHIF) approach ([64], https://bioinformatics.psb.ugent.be/plaza/versions/plaza_v4_dicots/,
399 supplemental table S6). GO term enrichment was performed in PLAZA 4.0 DICOT.

400

401 **Declarations**

402 *Competing interests*

403 The authors declare no conflicts of interest.

404

405 *Funding*

406 This work was funded by the Swedish Research Council VR (grant no. 2014-05822 to L.H.) and the
407 Swedish Research Council Formas (grant no. 2016-00961 to L.H.) and a grant from the Knut and Alice
408 Wallenberg foundation (grant no. 2012.0087 to L.H.).

409

410 *Acknowledgements*

411 The computations of the RNA-seq data were performed on resources provided by SNIC through the
412 Uppsala Multidisciplinary Center for Advanced Computational Science (UPPMAX) under Project SNIC
413 2017/7-6. We would like to thank Frédéric Berger (GMI) for kindly providing *Marchantia* H2A
414 antibodies.

415

416 *Author contributions*

417 L.H., C.K. and S.L. conceived the study. S.L. performed the experimental work. S.L., M.S.T.-A. and Y.Q.
418 performed the computational analysis. D.M.E. provided support to the experimental work. S.L. and C.K.
419 interpreted the data and wrote the manuscript. All authors approved the final version of the manuscript.

420

421 *Availability of data and materials*

422 The datasets supporting the conclusions of this article are available in the Gene Expression Omnibus
423 (GEO) with the accession number GSE164394.

424

425 **References**

426 1. Di Croce L, Helin K. Transcriptional regulation by Polycomb group proteins. *Nat Struct Mol Biol*. Nature
427 Publishing Group; 2013;20:1147–55.

428 2. Schwartz YB, Pirrotta V. A new world of Polycombs: unexpected partnerships and emerging functions.
429 *Nat Rev Genet*. Nature Publishing Group; 2013;14:853–64.

430 3. Mozgova I, Hennig L. The Polycomb Group Protein Regulatory Network. *Annu Rev Plant Biol*. Annual
431 Reviews; 2015;66:269–96.

432 4. Schuettengruber B, Bourbon H-M, Di Croce L, Cavalli G. Genome Regulation by Polycomb and
433 Trithorax: 70 Years and Counting. *Cell*. 2017;171:34–57.

434 5. Francis NJ, Kingston RE, Woodcock CL. Chromatin Compaction by a Polycomb Group Protein Complex.
435 *Science*. American Association for the Advancement of Science; 2004;306:1574–7.

436 6. Bratzel F, López-Torrejón G, Koch M, Del Pozo JC, Calonje M. Keeping Cell Identity in Arabidopsis
437 Requires PRC1 RING-Finger Homologs that Catalyze H2A Monoubiquitination. *Curr Biol*. 2010;20:1853–9.

438 7. Eskeland R, Leeb M, Grimes GR, Kress C, Boyle S, Sproul D, et al. Ring1B Compacts Chromatin
439 Structure and Represses Gene Expression Independent of Histone Ubiquitination. *Mol Cell*.
440 2010;38:452–64.

441 8. Xiao J, Wagner D. Polycomb repression in the regulation of growth and development in Arabidopsis.
442 *Curr Opin Plant Biol*. 2015;23:15–24.

443 9. Cao R, Wang L, Wang H, Xia L, Erdjument-Bromage H, Tempst P, et al. Role of Histone H3 Lysine 27
444 Methylation in Polycomb-Group Silencing. *Science*. American Association for the Advancement of
445 Science; 2002;298:1039–43.

446 10. Czermin B, Melfi R, McCabe D, Seitz V, Imhof A, Pirrotta V. Drosophila Enhancer of Zeste/ESC
447 Complexes Have a Histone H3 Methyltransferase Activity that Marks Chromosomal Polycomb Sites. *Cell*.
448 2002;111:185–96.

449 11. Kuzmichev A, Nishioka K, Erdjument-Bromage H, Tempst P, Reinberg D. Histone methyltransferase
450 activity associated with a human multiprotein complex containing the Enhancer of Zeste protein. *Genes*
451 *Dev*. 2002;16:2893–905.

452 12. Müller J, Hart CM, Francis NJ, Vargas ML, Sengupta A, Wild B, et al. Histone Methyltransferase
453 Activity of a Drosophila Polycomb Group Repressor Complex. *Cell*. 2002;111:197–208.

454 13. Gao Z, Zhang J, Bonasio R, Strino F, Sawai A, Parisi F, et al. PCGF Homologs, CBX Proteins, and RYBP
455 Define Functionally Distinct PRC1 Family Complexes. *Mol Cell*. 2012;45:344–56.

456 14. Hauri S, Comoglio F, Seimiya M, Gerstung M, Glatter T, Hansen K, et al. A High-Density Map for
457 Navigating the Human Polycomb Complexome. *Cell Rep*. 2016;17:583–95.

458 15. Wang H, Wang L, Erdjument-Bromage H, Vidal M, Tempst P, Jones RS, et al. Role of histone H2A
459 ubiquitination in Polycomb silencing. *Nature*. Nature Publishing Group; 2004;431:873–8.

460 16. Shao Z, Raible F, Mollaaghataba R, Guyon JR, Wu C, Bender W, et al. Stabilization of Chromatin
461 Structure by PRC1, a Polycomb Complex. *Cell*. 1999;98:37–46.

462 17. Francis NJ, Saurin AJ, Shao Z, Kingston RE. Reconstitution of a Functional Core Polycomb Repressive
463 Complex. *Mol Cell*. 2001;8:545–56.

464 18. Lo SM, Ahuja NK, Francis NJ. Polycomb Group Protein Suppressor 2 of Zeste Is a Functional Homolog
465 of Posterior Sex Combs. *Mol Cell Biol*. American Society for Microbiology Journals; 2009;29:515–25.

466 19. Xu L, Shen W-H. Polycomb Silencing of KNOX Genes Confines Shoot Stem Cell Niches in Arabidopsis.
467 *Curr Biol*. 2008;18:1966–71.

468 20. Bratzel F, Yang C, Angelova A, López-Torrejón G, Koch M, Pozo JC del, et al. Regulation of the New
469 Arabidopsis Imprinted Gene AtBMI1C Requires the Interplay of Different Epigenetic Mechanisms. *Mol
470 Plant*. Elsevier; 2012;5:260–9.

471 21. Yang C, Bratzel F, Hohmann N, Koch M, Turck F, Calonje M. VAL- and AtBMI1-Mediated H2Aub
472 Initiate the Switch from Embryonic to Postgerminative Growth in Arabidopsis. *Curr Biol*. 2013;23:1324–9.

473 22. Morey L, Aloia L, Cozzuto L, Benitah SA, Di Croce L. RYBP and Cbx7 Define Specific Biological
474 Functions of Polycomb Complexes in Mouse Embryonic Stem Cells. *Cell Rep*. 2013;3:60–9.

475 23. Tavares L, Dimitrova E, Oxley D, Webster J, Poot R, Demmers J, et al. RYBP-PRC1 Complexes Mediate
476 H2A Ubiquitylation at Polycomb Target Sites Independently of PRC2 and H3K27me3. *Cell*. 2012;148:664–
477 78.

478 24. Blackledge NP, Farcas AM, Kondo T, King HW, McGouran JF, Hanssen LLP, et al. Variant PRC1
479 Complex-Dependent H2A Ubiquitylation Drives PRC2 Recruitment and Polycomb Domain Formation. *Cell*.
480 2014;157:1445–59.

481 25. Endoh M, Endo TA, Endoh T, Isono K, Sharif J, Ohara O, et al. Histone H2A Mono-Ubiquitination Is a
482 Crucial Step to Mediate PRC1-Dependent Repression of Developmental Genes to Maintain ES Cell
483 Identity. *PLOS Genet*. Public Library of Science; 2012;8:e1002774.

484 26. Cooper S, Dienstbier M, Hassan R, Schermelleh L, Sharif J, Blackledge NP, et al. Targeting Polycomb
485 to Pericentric Heterochromatin in Embryonic Stem Cells Reveals a Role for H2AK119u1 in PRC2
486 Recruitment. *Cell Rep*. 2014;7:1456–70.

487 27. Illingworth RS, Moffat M, Mann AR, Read D, Hunter CJ, Pradeepa MM, et al. The E3 ubiquitin ligase
488 activity of RING1B is not essential for early mouse development. *Genes Dev*. 2015;29:1897–902.

489 28. Blackledge NP, Fursova NA, Kelley JR, Huseyin MK, Feldmann A, Klose RJ. PRC1 Catalytic Activity Is
490 Central to Polycomb System Function. *Mol Cell*. 2020;77:857–874.e9.

491 29. Tamburri S, Lavarone E, Fernández-Pérez D, Conway E, Zanotti M, Manganaro D, et al. Histone
492 H2AK119 Mono-Ubiquitination Is Essential for Polycomb-Mediated Transcriptional Repression. *Mol Cell*.
493 2020;77:840–856.e5.

494 30. Pengelly AR, Kalb R, Finkl K, Müller J. Transcriptional repression by PRC1 in the absence of H2A
495 monoubiquitylation. *Genes Dev.* Cold Spring Harbor Laboratory Press; 2015;29:1487.

496 31. Kahn TG, Dorafshan E, Schultheis D, Zare A, Stenberg P, Reim I, et al. Interdependence of PRC1 and
497 PRC2 for recruitment to Polycomb Response Elements. *Nucleic Acids Res.* Oxford Academic;
498 2016;44:10132–49.

499 32. Tsuboi M, Kishi Y, Yokozeki W, Koseki H, Hirabayashi Y, Gotoh Y. Ubiquitination-Independent
500 Repression of PRC1 Targets during Neuronal Fate Restriction in the Developing Mouse Neocortex. *Dev
501 Cell.* 2018;47:758-772.e5.

502 33. Zhou Y, Romero-Campero FJ, Gómez-Zambrano Á, Turck F, Calonje M. H2A monoubiquitination in
503 *Arabidopsis thaliana* is generally independent of LHP1 and PRC2 activity. *Genome Biol.* 2017;18:69.

504 34. Kralemann LEM, Liu S, Trejo-Arellano MS, Muñoz-Viana R, Köhler C, Hennig L. Removal of H2Aub1 by
505 ubiquitin-specific proteases 12 and 13 is required for stable Polycomb-mediated gene repression in
506 *Arabidopsis*. *Genome Biol.* 2020;21.

507 35. Yin X, Romero-Campero FJ, de Los Reyes P, Yan P, Yang J, Tian G, et al. H2AK121ub in *Arabidopsis*
508 associates with a less accessible chromatin state at transcriptional regulation hotspots. *Nat Commun.*
509 Nature Publishing Group; 2021;12:315.

510 36. Derkacheva M, Liu S, Figueiredo DD, Gentry M, Mozgova I, Nanni P, et al. H2A deubiquitinases
511 UBP12/13 are part of the *Arabidopsis* polycomb group protein system. *Nat Plants.* Nature Publishing
512 Group; 2016;2:1–10.

513 37. Bowman JL, Kohchi T, Yamato KT, Jenkins J, Shu S, Ishizaki K, et al. Insights into Land Plant Evolution
514 Garnered from the *Marchantia polymorpha* Genome. *Cell.* 2017;171:287-304.e15.

515 38. Kawashima T, Lorković ZJ, Nishihama R, Ishizaki K, Axelsson E, Yelagandula R, et al. Diversification of
516 histone H2A variants during plant evolution. *Trends Plant Sci.* 2015;20:419–25.

517 39. Montgomery SA, Tanizawa Y, Galik B, Wang N, Ito T, Mochizuki T, et al. Chromatin Organization in
518 Early Land Plants Reveals an Ancestral Association between H3K27me3, Transposons, and Constitutive
519 Heterochromatin. *Curr Biol.* 2020;30:573-588.e7.

520 40. Sanchez-Pulido L, Devos D, Sung ZR, Calonje M. RAWUL: A new ubiquitin-like domain in PRC1 Ring
521 finger proteins that unveils putative plant and worm PRC1 orthologs. *BMC Genomics.* 2008;9:308.

522 41. Junco SE, Wang R, Gaipa JC, Taylor AB, Schirf V, Gearhart MD, et al. Structure of the Polycomb Group
523 Protein PCGF1 in Complex with BCOR Reveals Basis for Binding Selectivity of PCGF Homologs. *Structure.*
524 2013;21:665–71.

525 42. Gray F, Cho HJ, Shukla S, He S, Harris A, Boytsov B, et al. BMI1 regulates PRC1 architecture and
526 activity through homo- and hetero-oligomerization. *Nat Commun.* Nature Publishing Group;
527 2016;7:13343.

528 43. Wong SJ, Gearhart MD, Taylor AB, Nanyes DR, Ha DJ, Robinson AK, et al. KDM2B Recruitment of the
529 Polycomb Group Complex, PRC1.1, Requires Cooperation between PCGF1 and BCORL1. *Structure*.
530 2016;24:1795–801.

531 44. Chittcock EC, Latwiel S, Miller TCR, Müller CW. Molecular architecture of polycomb repressive
532 complexes. *Biochem Soc Trans*. Portland Press; 2017;45:193–205.

533 45. Lee H-G, Kahn TG, Simcox A, Schwartz YB, Pirrotta V. Genome-wide activities of Polycomb complexes
534 control pervasive transcription. *Genome Res*. 2015;25:1170–81.

535 46. Gómez-Zambrano Á, Merini W, Calonje M. The repressive role of *Arabidopsis* H2A.Z in transcriptional
536 regulation depends on AtBMI1 activity. *Nat Commun*. Nature Publishing Group; 2019;10:2828.

537 47. Frangini A, Sjöberg M, Roman-Trufero M, Dharmalingam G, Haberle V, Bartke T, et al. The Aurora B
538 Kinase and the Polycomb Protein Ring1B Combine to Regulate Active Promoters in Quiescent
539 Lymphocytes. *Mol Cell*. 2013;51:647–61.

540 48. van den Boom V, Maat H, Geugien M, Rodríguez López A, Sotoca AM, Jaques J, et al. Non-canonical
541 PRC1.1 Targets Active Genes Independent of H3K27me3 and Is Essential for Leukemogenesis. *Cell Rep*.
542 2016;14:332–46.

543 49. Kloet SL, Makowski MM, Baymaz HI, van Voorthuijsen L, Karemaker ID, Santanach A, et al. The
544 dynamic interactome and genomic targets of Polycomb complexes during stem-cell differentiation. *Nat
545 Struct Mol Biol*. Nature Publishing Group; 2016;23:682–90.

546 50. Cohen I, Zhao D, Bar C, Valdes VJ, Dauber-Decker KL, Nguyen MB, et al. PRC1 Fine-tunes Gene
547 Repression and Activation to Safeguard Skin Development and Stem Cell Specification. *Cell Stem Cell*.
548 2018;22:726-739.e7.

549 51. Gao Z, Lee P, Stafford JM, von Schimmelmann M, Schaefer A, Reinberg D. An AUTS2–Polycomb
550 complex activates gene expression in the CNS. *Nature Publishing Group*; 2014;516:349–54.

551 52. Linde A-M, Eklund DM, Kubota A, Pederson ERA, Holm K, Gyllenstrand N, et al. Early evolution of the
552 land plant circadian clock. *New Phytol*. 2017;216:576–90.

553 53. Ishizaki K, Nishihama R, Ueda M, Inoue K, Ishida S, Nishimura Y, et al. Development of Gateway
554 Binary Vector Series with Four Different Selection Markers for the Liverwort *Marchantia polymorpha*.
555 PLOS ONE. Public Library of Science; 2015;10:e0138876.

556 54. Sugano SS, Nishihama R, Shirakawa M, Takagi J, Matsuda Y, Ishida S, et al. Efficient CRISPR/Cas9-
557 based genome editing and its application to conditional genetic analysis in *Marchantia polymorpha*.
558 PLOS ONE. Public Library of Science; 2018;13:e0205117.

559 55. Eklund DM, Kanei M, Flores-Sandoval E, Ishizaki K, Nishihama R, Kohchi T, et al. An Evolutionarily
560 Conserved Abscisic Acid Signaling Pathway Regulates Dormancy in the Liverwort *Marchantia polymorpha*. *Curr Biol*. 2018;28:3691-3699.e3.

562 56. Dobin A, Davis CA, Schlesinger F, Drenkow J, Zaleski C, Jha S, et al. STAR: ultrafast universal RNA-seq
563 aligner. *Bioinformatics*. Oxford Academic; 2013;29:15–21.

564 57. Love MI, Huber W, Anders S. Moderated estimation of fold change and dispersion for RNA-seq data
565 with DESeq2. *Genome Biol.* 2014;15:550.

566 58. Villar CBR, Köhler C. Plant Chromatin Immunoprecipitation. In: Hennig L, Köhler C, editors. *Plant Dev*
567 *Biol Methods Protoc.* Totowa, NJ: Humana Press; 2010. p. 401–11. Available from:
568 https://doi.org/10.1007/978-1-60761-765-5_27

569 59. Bolger AM, Lohse M, Usadel B. Trimmomatic: a flexible trimmer for Illumina sequence data.
570 *Bioinformatics.* Oxford Academic; 2014;30:2114–20.

571 60. Langmead B, Salzberg SL. Fast gapped-read alignment with Bowtie 2. *Nat Methods.* Nature
572 Publishing Group; 2012;9:357–9.

573 61. Heinz S, Benner C, Spann N, Bertolino E, Lin YC, Laslo P, et al. Simple Combinations of Lineage-
574 Determining Transcription Factors Prime cis-Regulatory Elements Required for Macrophage and B Cell
575 Identities. *Mol Cell.* 2010;38:576–89.

576 62. Thorvaldsdóttir H, Robinson JT, Mesirov JP. Integrative Genomics Viewer (IGV): high-performance
577 genomics data visualization and exploration. *Brief Bioinform.* Oxford Academic; 2013;14:178–92.

578 63. Ramírez F, Dündar F, Diehl S, Grüning BA, Manke T. deepTools: a flexible platform for exploring
579 deep-sequencing data. *Nucleic Acids Res.* Oxford Academic; 2014;42:W187–91.

580 64. Van Bel M, Diels T, Vancaester E, Kreft L, Botzki A, Van de Peer Y, et al. PLAZA 4.0: an integrative
581 resource for functional, evolutionary and comparative plant genomics. *Nucleic Acids Res.* Oxford
582 Academic; 2018;46:D1190–6.

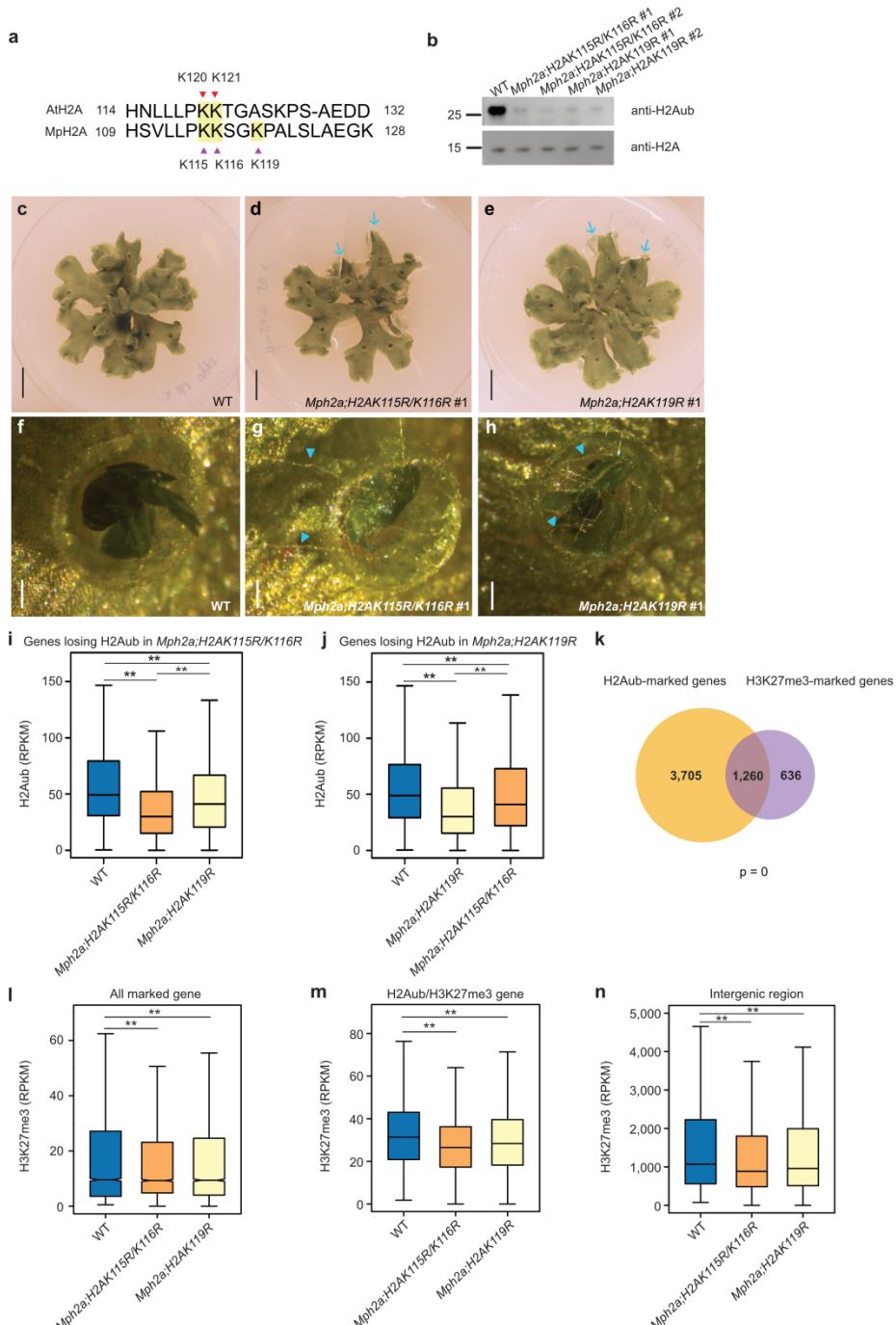
583

584

585

586

587



588

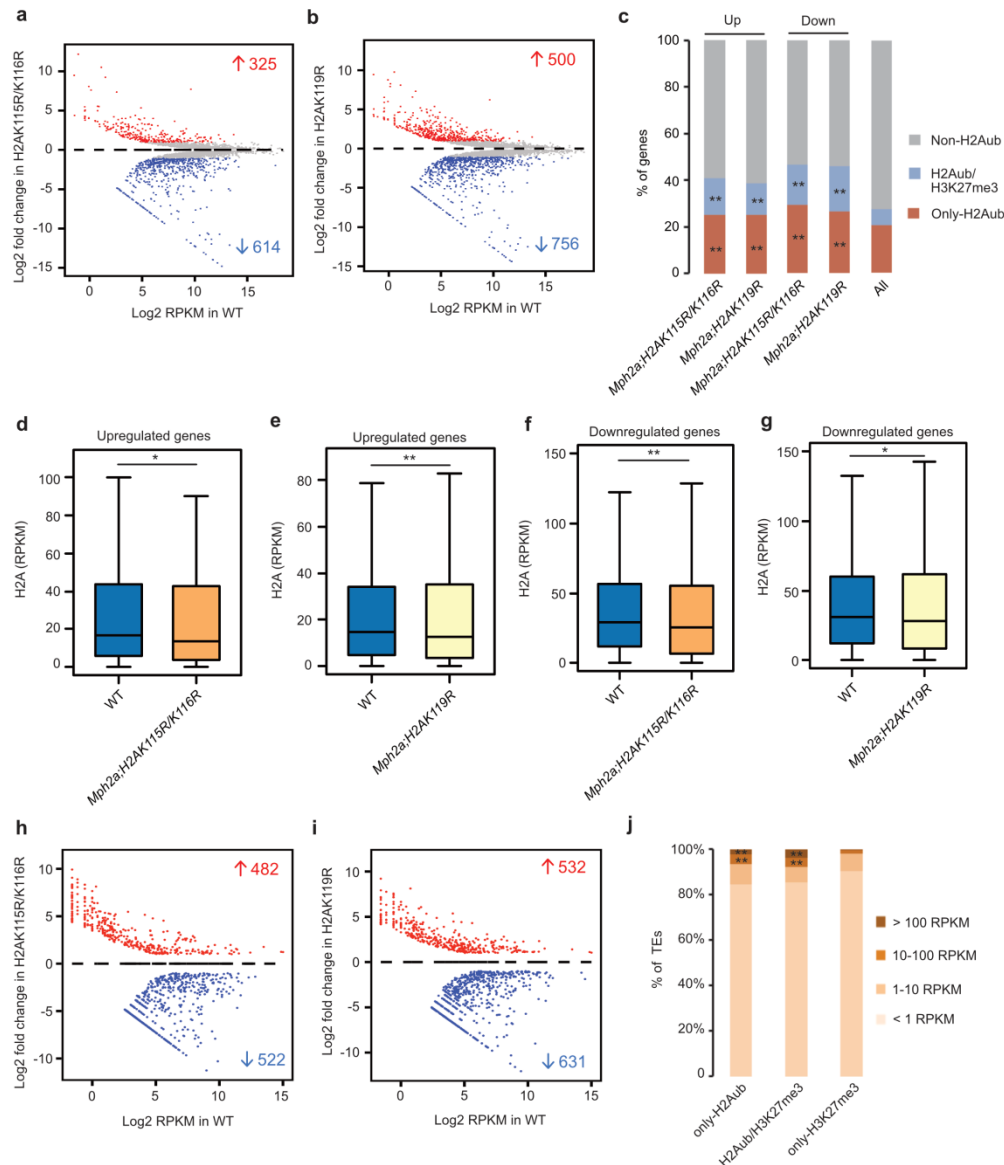
589

Fig. 1 H2Aub directly contributes to the deposition of H3K27me3

590 a. Lysine residues in *Arabidopsis* and *Marchantia* H2A. Lysine 120 (K120) and K121 of H2A in *Arabidopsis* and
591 potential ubiquitination sites (K115, K116 and K119) in H2A of *Marchantia* are highlighted. b. Western blot of bulk
592 H2Aub and H2A in wild type (WT), *Mph2a;H2AK115R/K116R* #1, *Mph2a;H2AK115R/K116R* #2,
593 *Mph2a;H2AK119R* #1 and *Mph2a;H2AK119R* #2 mutants. c-e. Phenotypes of 28 day-old WT,
594 *Mph2a;H2AK115R/K116R* #1 and *Mph2a;H2AK119R* #1 mutants. Blue arrows point to downward curled edges of
595 the thallus. Scale bars, 1 cm. f-h. Gemma cup phenotypes of WT, *Mph2a;H2AK115R/K116R* #1 and
596 *Mph2a;H2AK119R* #1 mutants. Blue arrowheads point to visible rhizoids produced by non-dormant gemmae in the
597 mutants. Scale bars, 0.05 cm. i. Boxplots showing H2Aub levels (RPKM, reads per kilobase per million mapped
598 reads) of genes losing H2Aub in *Mph2a;H2AK115R/K116R* in WT, *Mph2a;H2AK115R/K116R* and

599 *Mph2a;H2AK119R* mutants. j. Boxplots showing H2Aub levels of genes losing H2Aub in *Mph2a;H2AK119R* in
600 WT, *Mph2a;H2AK119R* and *Mph2a;H2AK115R/K116R* mutants. k. Venn diagram showing overlap of H2Aub-
601 marked genes and H3K27me3-marked genes in wild type (WT). Significance was tested using a Hypergeometric
602 test. l, m. Boxplots showing H3K27me3 levels of all marked genes (l) and H2Aub/H3K27me3 genes (m) in WT,
603 *Mph2a;H2AK115R/K116R* and *Mph2a;H2AK119R* mutants. H2Aub and H3K27me3 levels were calculated as the
604 average RPKM from 1 kb upstream of the transcriptional start to the transcriptional start of genes. n. Boxplot
605 showing H3K27me3 levels in intergenic regions marked by H2Aub and H3K27me3 in WT,
606 *Mph2a;H2AK115R/K116R* and *Mph2a;H2AK119R* mutants. Boxes show medians and the interquartile range, and
607 error bars show the full range excluding outliers. **, p < 0.01 (Wilcoxon test).

608
609
610
611
612
613
614
615
616
617
618
619
620



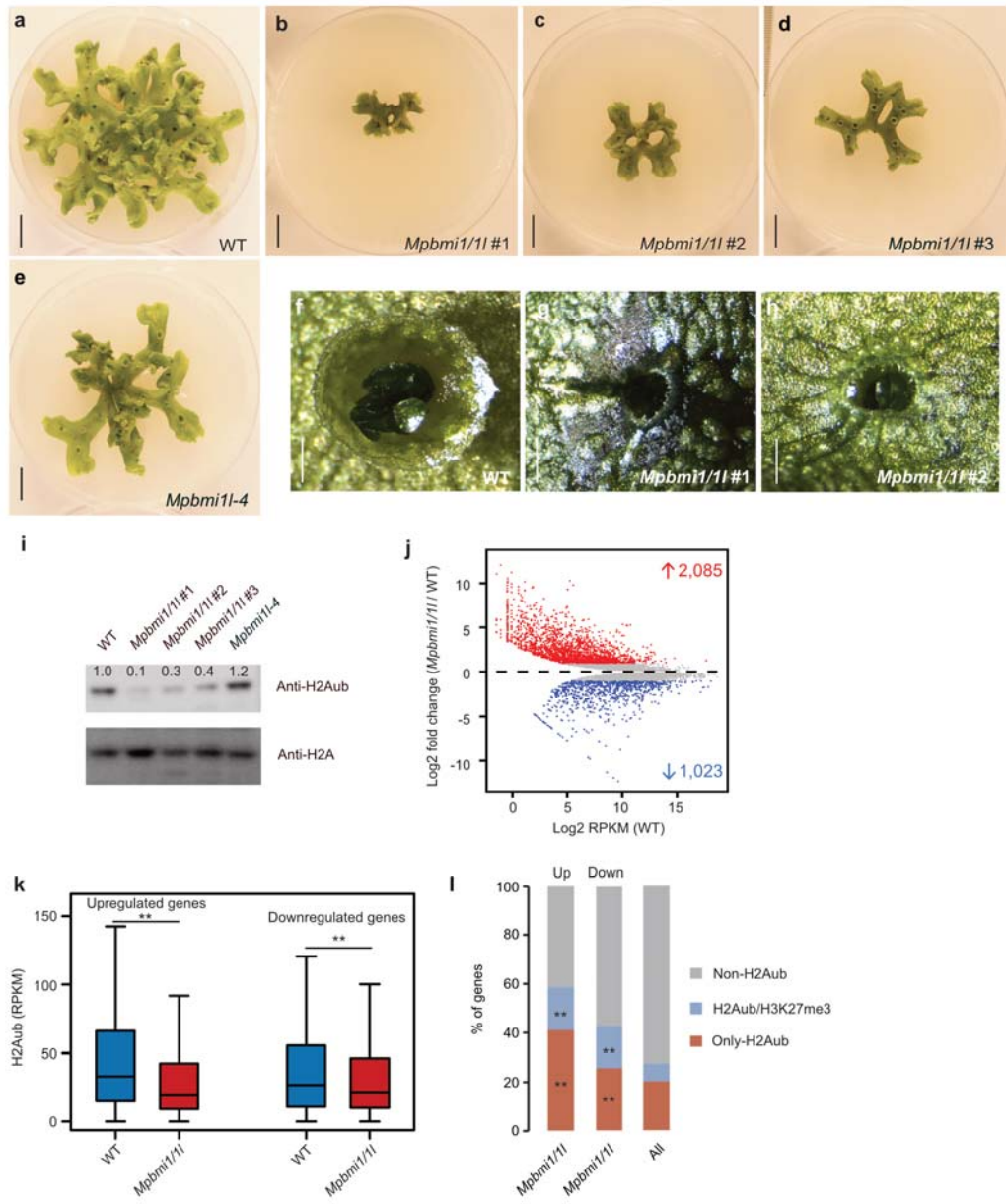
621

622

Fig. 2 H2Aub is required for gene activation

623
624
625
626
627
628
629
630
631
632
633
634
635
636
637

a, b. MA plots showing differential gene expression (Log2 fold change) in *Mph2a;H2AK115R/K116R* (a) and *Mph2a;H2AK119R* (b) mutants compared to wild type (WT). Significant changes are marked in red (log2 fold change ≥ 1 and adjusted p value ≤ 0.05) and blue (log2 fold change ≤ -1 and adjusted p value ≤ 0.05). c. Presence of only-H2Aub or H2Aub/H3K27me3 marks on upregulated (Up) and downregulated (Down) genes in *Mph2a;H2AK115R/K116R* and *Mph2a;H2AK119R* mutants. Presence of modifications is based on their distribution in WT. **, p < 0.01 (Hypergeometric test). d, e. Boxplots showing the H2Aub level on upregulated genes in *Mph2a;H2AK115R/K116R* (d) and *Mph2a;H2AK119R* (e) mutants. f, g. Boxplots showing H2Aub level on downregulated genes in *Mph2a;H2AK115R/K116R* (f) and *Mph2a;H2AK119R* (g) mutants. H2Aub levels were calculated as the average RPKM from 1 kb upstream of the transcriptional start to the transcriptional start of genes. Boxes show medians and the interquartile range, and error bars show the full range excluding outliers. **, p < 0.01 (Wilcoxon test). h, i. MA plots showing differential expression of transposable elements (TEs) (Log2 fold change) in *Mph2a;H2AK115R/K116R* (h) and *Mph2a;H2AK119R* (i) mutants. Significant gene expression changes are marked in red (log2 fold change ≥ 1 and adjusted p value ≤ 0.05) and blue (log2 fold change ≤ -1 and adjusted p value ≤ 0.05). j. Expression level distribution of transposable elements (TEs) marked by only-H2Aub, H2Aub/H3K27me3 and only-H3K27me3 in WT. **, p < 0.01 (Hypergeometric test).

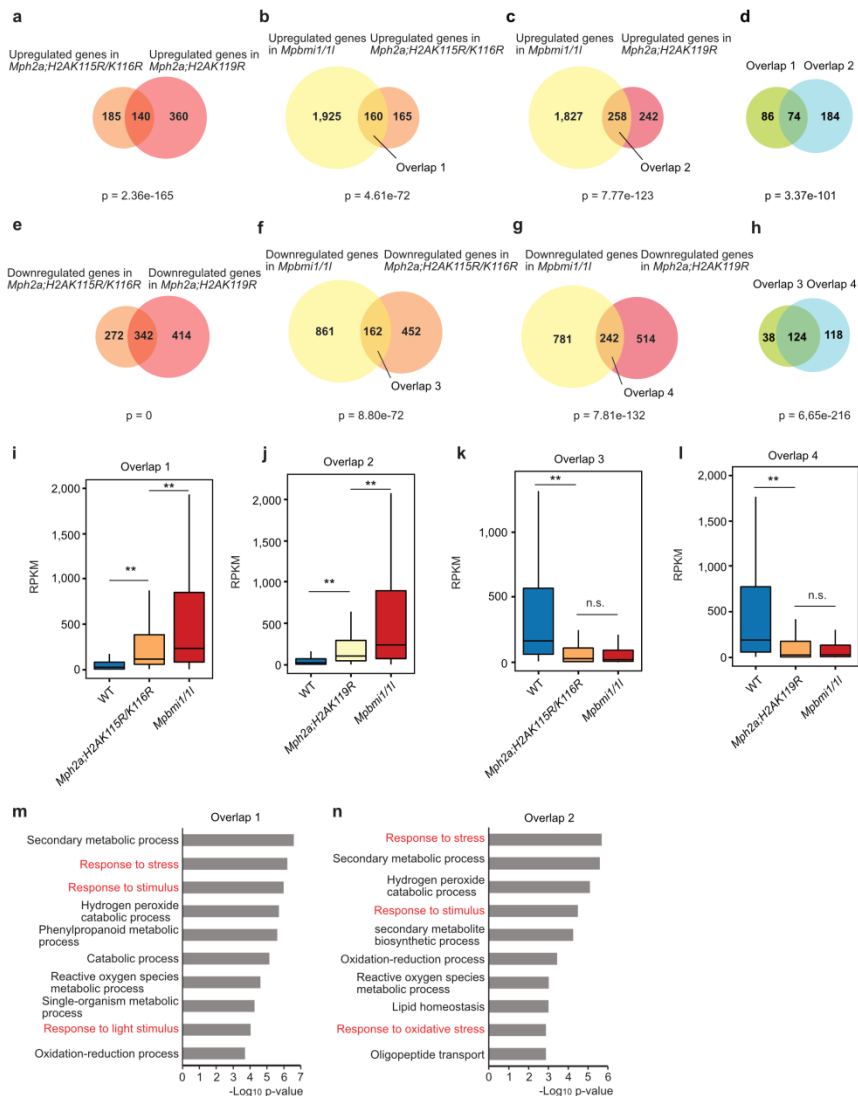


638

639 **Fig. 3 MpBMI1/1L affect morphological development of *Marchantia* and regulate gene silencing and**

640 activation

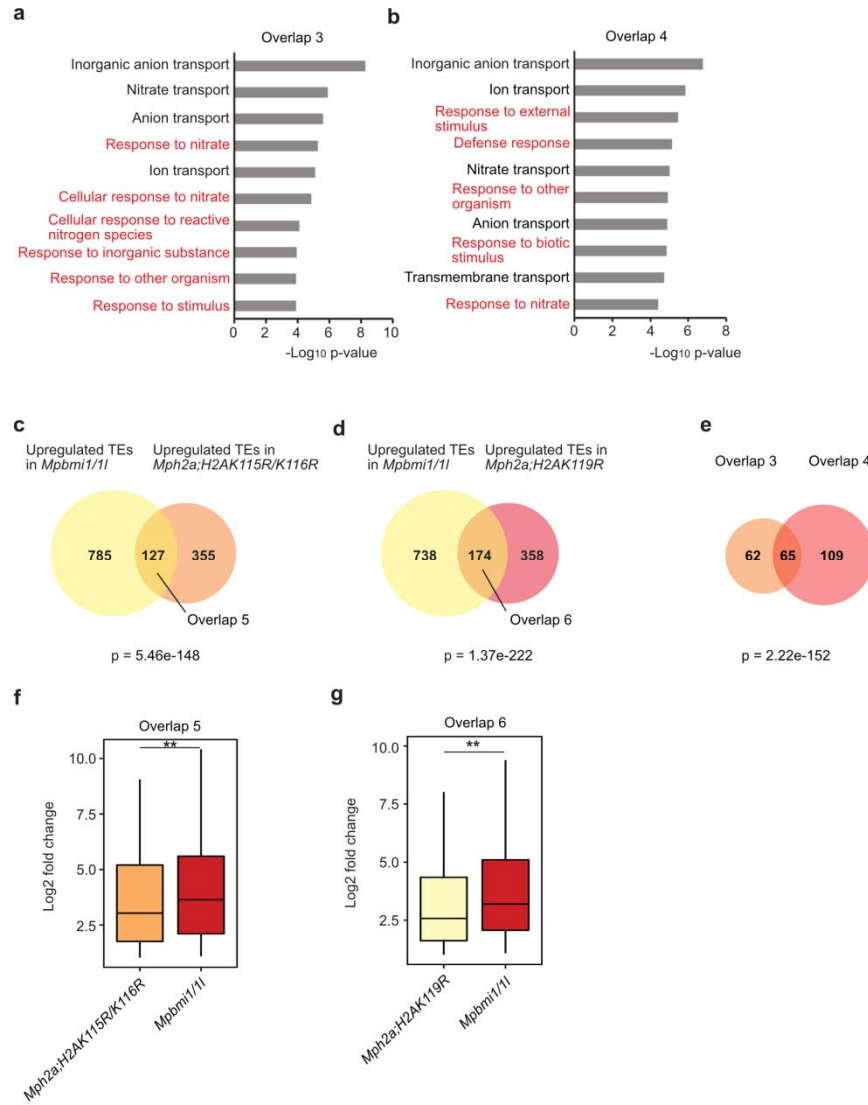
641 a-e. Morphological phenotypes of 35 day-old wild type (WT), *Mpbmi1/1l* #1, *Mpbmi1/1l* #2, *Mpbmi1/1l* #3 and
 642 *Mpbmi1/1l*-4 lines. Scale bars: 1 cm. f-h. Gemma cups of 35 day-old WT, *Mpbmi1/1l* #1 and *Mpbmi1/1l* #2 lines.
 643 Scale bars: 0.1 cm. i. Western blot showing the bulk H2Aub levels in WT, *Mpbmi1/1l* #1, *Mpbmi1/1l* #2, *Mpbmi1/1l*
 644 #3 and *Mpbmi1/1l*-4 mutants. j. MA plot showing differential gene expression (Log2 fold change) in *Mpbmi1/1l* #1
 645 mutants compared to WT. Significant gene expression changes are marked in red (log2 fold change ≥ 1 and adjusted
 646 p value ≤ 0.05) and blue (log2 fold change ≤ -1 and adjusted p value ≤ 0.05). i. Boxplot showing the H2Aub level
 647 (RPKM, reads per kilobase per million mapped reads) of upregulated and downregulated genes in *Mpbmi1/1l* #1
 648 mutants. H2Aub levels were calculated as the average RPKM from 1 kb upstream of the transcriptional start to the
 649 transcriptional start of genes. Boxes show medians and the interquartile range, and error bars show the full range
 650 excluding outliers. **, p < 0.01 (Wilcoxon test). j. Percent of upregulated (Up) and downregulated (Down) genes
 651 marked by only-H2Aub and H2Aub/H3K27me3 in *Mpbmi1/1l* #1 mutants. **, p < 0.01 (Hypergeometric test).



652

Fig. 4 H2Aub contributes to PRC1-mediated transcriptional expression

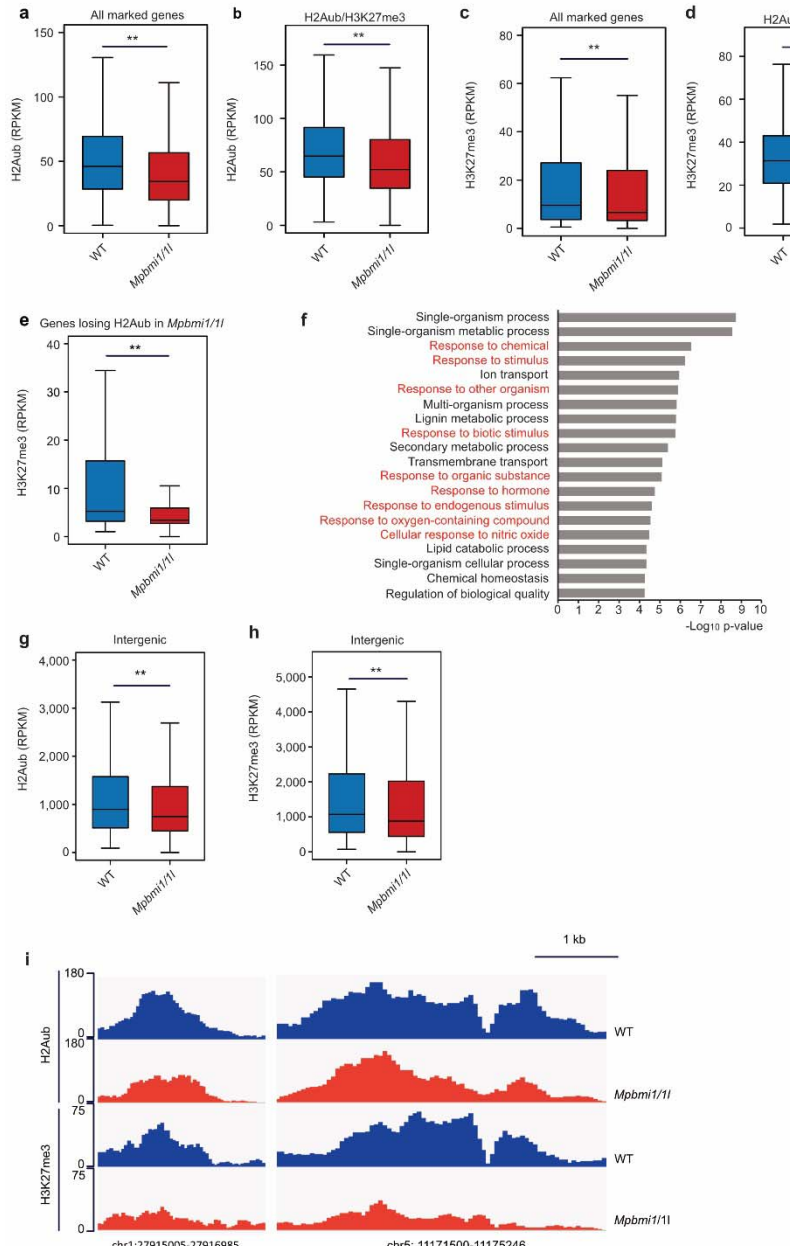
653 a. Venn diagram showing overlap of upregulated genes in *Mph2a;H2AK115R/K116R* and *Mph2a;H2AK119R* mutants. Significance was tested using a Hypergeometric test. b. Venn diagram showing overlap of upregulated genes in *Mpbmi1/1l* mutants and *Mph2a;H2AK115R/K116R* mutants. c. Venn diagram showing overlap of upregulated genes in *Mpbmi1/1l* mutants and *Mph2a;H2AK119R* mutants. d. Venn diagram showing overlap of commonly upregulated genes in overlap 1 (panel b) and overlap 2 (panel c). e. Venn diagram showing overlap of downregulated genes in *Mph2a;H2AK115R/K116R* and *Mph2a;H2AK119R* mutants. f. Venn diagram showing overlap of downregulated genes in *Mpbmi1/1l* mutants and *Mph2a;H2AK115R/K116R* mutants. g. Venn diagram showing overlap of downregulated genes in *Mpbmi1/1l* mutants and *Mph2a;H2AK119R* mutants. h. Venn diagram showing overlap of commonly downregulated genes in overlap 3 (panel f) and overlap 4 (panel g). i. Boxplot showing expression level (RPKM, reads per kilobase per million mapped reads) of genes in overlap 1 (panel b) in WT, *Mph2a;H2AK115R/K116R* and *Mpbmi1/1l*. j. Boxplot showing expression level (RPKM) of genes in overlap 2 (panel c) in WT, *Mph2a;H2AK119R* and *Mpbmi1/1l*. k. Boxplot showing expression level (RPKM, reads per kilobase per million mapped reads) of genes in overlap 3 (panel f) in WT, *Mph2a;H2AK115R/K116R* and *Mpbmi1/1l*. l. Boxplot showing expression level (RPKM) of genes in overlap 4 (panel g) in WT, *Mph2a;H2AK119R* and *Mpbmi1/1l*. Boxes show medians and the interquartile range, and error bars show the full range excluding outliers. **, $p < 0.01$ (Wilcoxon test). m, n. Enriched GO terms of commonly upregulated genes in overlap 1 (panel b) and overlap 2 (panel c). Response pathways are marked in red.



671

672 **Fig. 5 H2Aub is essential in PRC1-mediated transposable element silencing**

673 a, b. Enriched GO terms of commonly downregulated genes in overlap 3 (panel f in Fig. 4) and overlap 4 (panel g in
674 Fig. 4). Response pathways are marked in red. c. Venn diagram showing overlap of upregulated transposable
675 elements (TEs) in *Mpbmi1/1l* and *Mph2a;H2AK115R/K116R* mutants. Significance was tested using a
676 Hypergeometric test. d. Venn diagram showing overlap of upregulated TEs in *Mpbmi1/1l* and *Mph2a;H2AK119R*
677 mutants. Significance was tested using a Hypergeometric test. e. Venn diagram showing overlap of commonly
678 upregulated TEs in overlap 5 (panel c) and overlap 6 (panel d). f. Boxplot showing differential expression level
679 (Log₂ fold change) of TEs in overlap 5 (panel c) in *Mph2a;H2AK115R/K116R* and *Mpbmi1/1l* mutants compared to
680 WT. n. Boxplot showing differential expression level (Log₂ fold change) of TEs in overlap 6 (panel d) in
681 *Mph2a;H2AK119R* and *Mpbmi1/1l* mutants compared to WT. Boxes show medians and the interquartile range, and
682 error bars show the full range excluding outliers. **, p < 0.01 (Wilcoxon test).



683
684

685 **Fig. 6 H3K27me3 is decreased on Polycomb target genes in genic and intergenic region by depletion of**
686 ***MpBMI1/1L***

687 a, b. Boxplots showing H2Aub level (RPKM, reads per kilobase per million mapped reads) on all marked genes (a)
688 and H2Aub/H3K27me3 genes (b) in WT and *Mpbmi1/1L* mutants. c, d. Boxplots showing H3K27me3 level on all
689 marked genes (c) and H2Aub/H3K27me3 genes (d) in WT and *Mpbmi1/1L* mutants. H2Aub and H3K27me3 levels
690 were calculated as the average RPKM from 1 kb upstream of the transcriptional start to the transcriptional start of
691 genes. e. Boxplot showing H3K27me3 level of genes with reduced H2Aub level in *Mpbmi1/1L* mutants. f. GO terms
692 of genes with reduced H2Aub level in *Mpbmi1/1L* mutants. Response pathways are marked in red. g, h. Boxplots
693 showing H2Aub (g) and H3K27me3 level (h) on H2Aub/H3K27me3-occupying intergenic regions in wild type (WT)
694 and *Mpbmi1/1L* mutants. Boxes show medians and the interquartile range, and error bars show the full range
695 excluding outliers. **, p < 0.01 (Wilcoxon test). i. Genome browser views of two selected intergenic loci showing
696 decreased H2Aub and H3K27me3 marks in *Mpbmi1/1L* mutants compared to WT.